

pubs.acs.org/Macromolecules Article

Ion Specific, Thin Film Confinement Effects on Conductivity in Polymerized Ionic Liquids

Qiujie Zhao, Peter Bennington, Paul F. Nealey, Shrayesh N. Patel,* and Christopher M. Evans*



Cite This: *Macromolecules* 2021, 54, 10520–10528



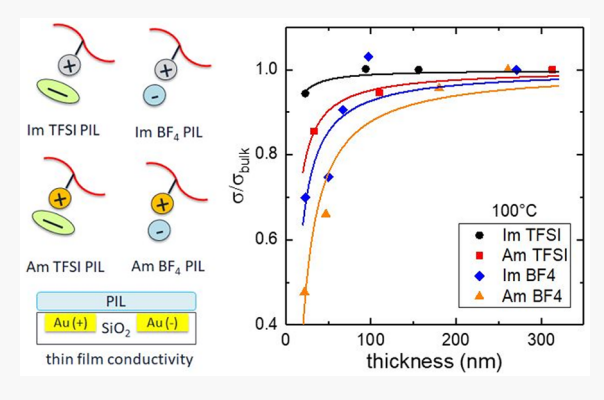
ACCESS

Metrics & More

Article Recommendations

Supporting Information

ABSTRACT: Acrylate-based polymerized ionic liquids (PILs) with ammonium (Am) or imidazolium (Im) cations and tetrafluoroborate (BF₄) or bis(trifluoromethanesulfonyl)imide (TFSI) anions were synthesized and spin coated onto gold interdigitated electrodes on silica to investigate nanoconfinement effects on ion transport. The film thickness ranged from 23 to 313 nm. A significant reduction of the inplane conductivity was observed in some PIL thin films with thickness below 100 nm. Specifically, Am BF₄ PIL showed the largest conductivity drop (ca. 50% difference between a 22 nm and a 261 nm film) while Im TFSI PIL showed almost no change under confinement. The difference in conductivity drop is discussed in terms of (i) differences in interfacial layer thickness by fitting a two-layer conductivity model and (ii) potential changes in glass transition temperature (T_g) under confinement, which



were estimated using the Vogel-Fulcher-Tammann fits of bulk conductivities. Decreasing film thickness also caused the dielectric loss peaks to shift to lower frequency, indicating that the ion diffusion process slowed under confinement.

■ INTRODUCTION

Polymerized ionic liquids (PILs) are a novel class of ionic polymers where ionic liquid (IL) moieties are covalently attached to a polymer backbone. These materials have excellent thermal and electrochemical stability, good ionic conductivity, tunable mechanical properties, and a wide design space due to the abundant choices of IL species and polymer matrices. 1,2 Recent works have investigated PILs as polymer electrolytes in energy applications including batteries,^{3,4} supercapacitors^{5,6} and ionic acutators.^{7,8} However, ion transport in polymer electrolytes is slower than that in smallmolecule liquid electrolytes due to the coupling with polymer segmental dynamics. To address this problem, various strategies have been explored to decouple ion and segmental motion and enhance ionic conductivity, such as tuning the IL species, 10,11 charge placement, 12,13 polymer backbone, 14-16 and side chain chemistry.¹⁷ In this work, we are focusing on the confinement effect on ion transport in PILs and trying to understand the structure-conductivity relationships in PIL thin films.

Confinement is a good strategy to modify the polymer and ion dynamics in PILs, and numerous works have studied the confinement on small-molecule ILs, 18-21 which revealed the importance of surface interactions and provided insight into PIL confinement. Common methodologies include the uses of nanostructured block copolymers, nanoporous templates, or nanothin films. 22 The block copolymer strategy typically uses a PIL block for ion conduction and a neutral polymer block for mechanical robustness. Segalman and co-workers 23 reported a

proton and bis(trifluoromethanesulfonyl)imide (TFSI) dualion conducting polystyrene-b-PIL with a lamellar morphology and enhanced conductivity. The enhancement was attributed to less ion aggregation upon confinement and to changes in chain conformations near the block copolymer interface. Ye et al. 24 designed a poly(methylmethacrylate)-based diblock copolymer with tethered imidazolium cations and mobile TFSI anions, and the material showed an almost 2 orders of magnitude increase in conductivity compared to a random copolymer with a similar PIL composition. Subsequent work on the same block copolymer but with bromide anions²⁵ exhibited a well-ordered lamellar morphology and a higher conductivity at 90% relative humidity than the PIL homopolymer, which was attributed to ion-water confinement effects in nanochannels. In contrast, some PIL block copolymers have conductivity lower than the homo-PIL due to the nonconductive block. Even after accounting for the PIL volume fraction, 26,27 the normalized ionic conductivity of the PIL block copolymer can be smaller (i.e., $\sigma_{
m block-PIL}/$ $\phi_{\text{PIL}}\sigma_{\text{homo-PIL}}$ < 1) due to tortuosity of the self-assembled morphologies. In addition, confinement can be achieved by

Received: August 28, 2021
Revised: October 18, 2021
Published: November 8, 2021





Scheme 1. Synthesis of Pendant Acrylate PILs with Varying Cations (Imidazolium or Ammonium) and Anions (BF4 or TFSI)

filling cylindrical nanopores with a PIL. This was recently demonstrated by polymerizing vinyl imidazolium (Im) TFSI monomer in silica nanopores²⁸ and nanoporous aluminum oxide (AO) membranes.²⁹ In the latter case, the confined PIL showed higher molecular weight than the bulk-synthesized polymer due to restricted chain motion and less termination. The PIL conductivity was enhanced by confinement, and it was attributed to the spatial heterogeneity of polymer dynamics in the nanopores (i.e., the conductivity relaxation is much faster at the center of the nanopores than in the bulk). The conductivity enhancement increased with reducing pore size, and confined PILs were able to achieve similar and even higher conductivity than the bulk IL monomer at low temperatures.

The thin film confinement is the focus of this study, and we note that conductivity measurements on PIL thin films have been demonstrated in through-plane configuration. Heres et al.³⁰ investigated a series of poly(1-ethyl-3-vinylimidazolium) TFSI PIL films with thickness ranging from 7.5 to 60 nm on silica using nanostructured parallel plate electrodes, but they needed to add an air gap between the polymer and the top electrode to prevent a short circuit. As a result, the impedance of air needed to be considered during analysis. The "mean ion dynamic rate", defined as the peak frequency in the dielectric loss spectra, was compared among PILs with different thicknesses and was unaffected by confinement below the glass transition temperature but systematically decreased with decreasing film thickness above T_g . This was rationalized in terms of the surface-polymer interaction where the negatively charged silica surface attracted the polycation chains and restricted ion motion above T_g due to strong coupling between mobile anions and the polymer backbone. Below T_g , the anion motion dominated the measured ion dynamics and was less affected by the film thickness. The slowdown of ion motion under confinement was also confirmed by molecular dynamic simulations³¹ of a 5 nm poly(1-butyl-3-vinylimidazolium) hexafluorophosphate (PF₆) PIL thin film on quartz where the anion hopping was much slower at the interface than in the

The studies mentioned above are of great value for understanding the fundamentals of ion transport in PILs and guiding polymer electrolyte development as well as interface engineering. Yet, the range of materials studied thus far is limited, and most studies focused on one specific PIL chemistry. It is an open question how changing the ionic interaction strength and polymer dynamics affects ion transport under confinement. To address this point, we systematically tuned the ionic interactions by synthesizing four PILs with different ion pairs, ammonium or imidazolium cations with tetrafluoroborate (BF₄) or TFSI anions, and investigated their conductivity-thickness-temperature relationships using interdigitated electrodes (IDE) as an in-plane measurement platform. IDE avoided the additional impedance from the air gap compared to the work of Heres et al.³⁰ and simplified the data analysis. We found that PIL conductivity started to decrease when the thin film thickness was less than 100 nm. The ammonium (Am) BF₄ PIL showed an approximately 50% conductivity drop while the Im TFSI PIL showed only a 6% decrease at 100 °C. The conductivityconfinement trend is the following: Im TFSI < Am TFSI < Im BF₄ < Am BF₄. The conductivity-thickness relationship was also fit to a two-layer model, and the results suggest that the interfacial layer thickness depends on the ionic interaction strength. A T_g increase in the PIL thin films may also occur as thickness decreases due to stronger interactions between the polymer and the substrate. The VFT dependence of the PILs was analyzed, and the conductivity fragility (m_{cond}) was determined. It was found that PILs with a lower $m_{\rm cond}$ showed greater confinement effects on the measured conductivity. Finally, the peaks in the dielectric loss $(\tan(\delta))$ spectra of PILs all shifted to lower frequency as film thickness decreased, suggesting the slowdown of ion diffusion under nanoconfinement.

■ RESULTS AND DISCUSSION

The synthetic route of pendant PILs with an acrylate backbone is shown in Scheme 1. To start, 3-bromo-1-propanol was first converted into a 3-bromopropyl acrylate via a facile reaction with acryloyl chloride. The bromine end was used to quanternize 1-methyl imidazole or *N*,*N*-dimethylbutylamine to form the imidazolium or ammonium cations. The Im or Am Br IL monomer was then polymerized by reversible addition—fragmentation chain transfer (RAFT) polymerization to prepare Im or Am Br PILs with high molecular weight and low polydispersity. Finally, the Br PILs were ion exchanged to

Table 1. Summary of PIL's Bulk $T_{\rm g}$ from DSC, VFT Fit Parameters for Conductivities of the Thickest PIL Films, Conductivity Fragility ($m_{\rm cond}$), Slopes of VFT Curves (s) at $T_{\rm g}/T=0.8$, and Interfacial Layer Thickness ($h_{\rm int}$) at 100 °C Based on a Bilayer Model

PIL sample	$T_{\rm g,bulk}$ (K)	h (nm)	σ_{∞} (S/cm)	T_0 (K)	$T_{\rm g,bulk} - T_0$ (K)	D	$m_{\rm cond}$	VFT slope $s (T_g/T = 0.8)$	$h_{\rm int}$ (nm)
Im TFSI	260	156	0.22	222 ± 4	38	4.2 ± 0.4	71 ± 17	15	1.2 ± 0.3
Im BF ₄	298	271	47	214 ± 6	84	11 ± 1	42 ± 8	18	7.3 ± 1.5
Am TFSI	268	313	0.14	230 ± 3	38	3.8 ± 0.3	70 ± 13	14	4.8 ± 0.4
Am BF ₄	306	261	12	211 ± 14	95	11 ± 3	33 ± 14	16	12.2 ± 1.2

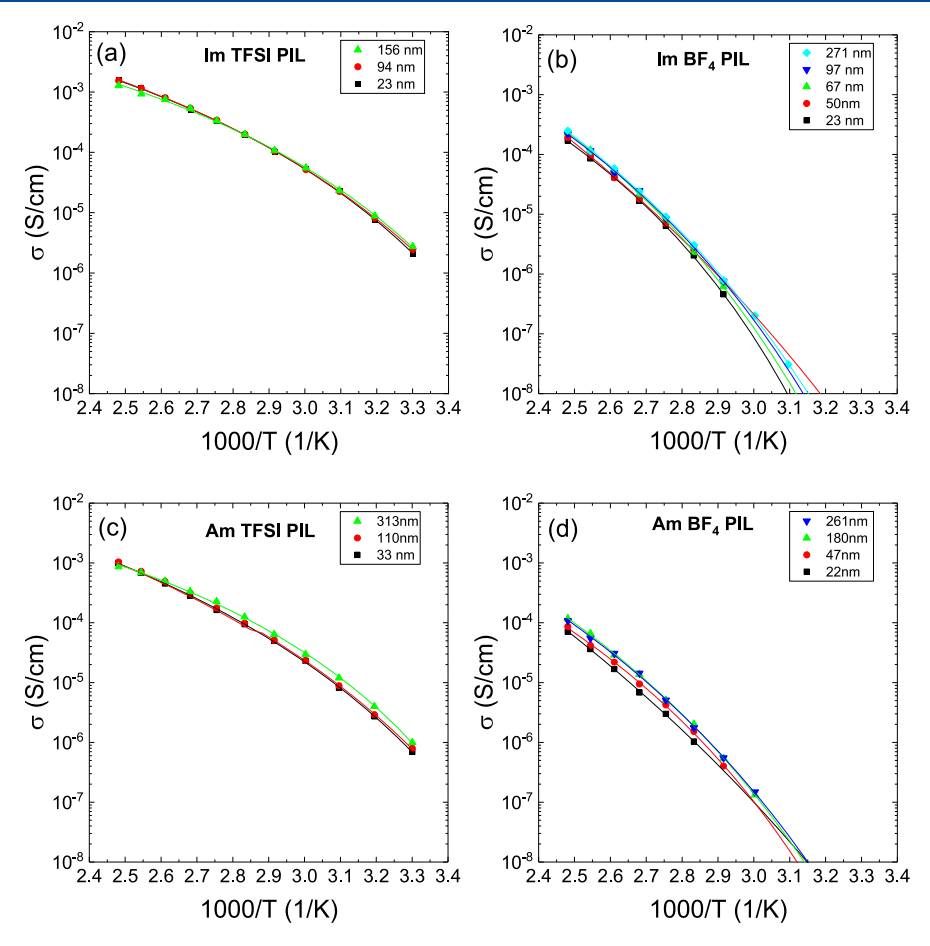


Figure 1. Conductivity vs 1000/T at various film thickness for (a) Im TFSI PIL, (b) Im BF₄ PIL, (c) Am TFSI PIL, and (d) Am BF₄ PIL. The solid lines are VFT fits.

either BF4 or TFSI anions using 10 equiv of NaBF4 or LiTFSI salts and dialyzing against either 1:1 (v/v) methanol-water mixture or pure water in a dialysis bag for 5 days to remove residue Br anions and excess salt. The conditions for ion exchange were shown to be sufficient in prior work, 32 and the elemental analysis confirmed that the residual bromide contents for the four PILs were < 0.7 wt % (Table S1). The Im TFSI PIL sample with a number-average degree of polymerization determined by nuclear magnetic resonance $(N_{\rm NMR})$ of 290 was used from the previous study.³³ The Im BF₄ PIL was synthesized from a separate batch of Br PIL with N_{NMR} = 110 (Figure S1a). The Am TFSI and Am BF₄ PILs were converted from the same batch of Am Br PIL and have $N_{\rm NMR}$ = 104 and 105, respectively (Figure S1b and c). The molecular weight effect on bulk ionic conductivity is negligible at a high degree of polymerization (N > 100). ^{33,34} However, it is still possible that molecular weight scaling of dynamic properties can be altered under nanoconfinement, which has been demonstrated in neutral polymers.³⁵

Bulk glass transition temperatures $(T_{\rm g,bulk})$ of the four PILs measured by differential scanning calorimetry (DSC) are shown in Table 1 and Figure S2. The systematic increases in $T_{\rm g}$ when switching from TFSI to BF₄ anions and from imidazolium to ammonium cations are consistent with previous research. ^{36,37}

Preparing ionic polymer thin films by spin coating requires careful choice of solvent as most polar solvents have high boiling points (e.g., water, dimethylsulfoxide, dimethylformamide), which are not ideal for fast solvent evaporation during spinning. Acetonitrile was chosen in this study due to its low boiling point, good PIL solubility, and ability to produce smooth films (Figure S3). The PIL thin film conductivity was collected by measuring the in-plane impedance of spin-coated films on interdigitated gold electrodes fabricated on Si wafers. ^{38,39} The gold electrode array consisted of N=160 individual electrodes each with length l=1 mm and width w=2 μ m. The electrode spacing was d=8 μ m. The film resistance

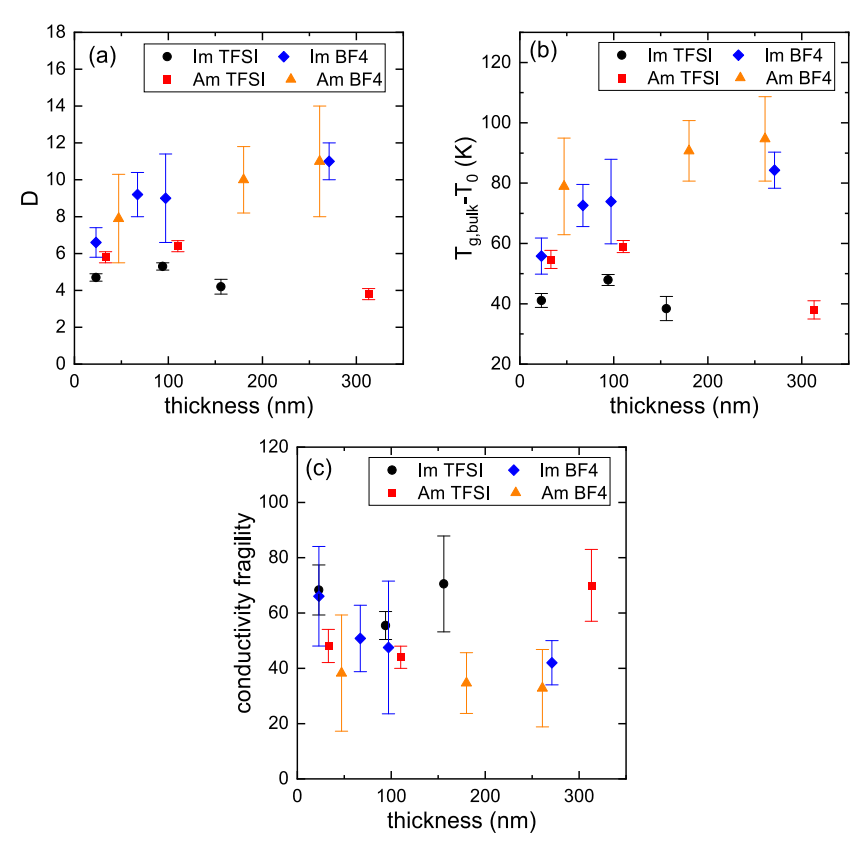


Figure 2. (a) Strength parameter D, (b) $T_{\rm g,bulk} - T_{\rm 0}$, and (c) calculated conductivity fragility from the VFT fits as a function of film thickness for four PILs. The error bars indicate the uncertainties from the fitting.

(R_f) was extracted by fitting the impedance spectra with an equivalent circuit, and the ionic conductivity was calculated as

$$\sigma = \frac{1}{R_{\rm f}} \frac{d}{(N-1)lh} \tag{1}$$

where *h* is the film thickness measured by ellipsometry. The effect of temperature on PIL thin film conductivity is shown in Figure 1. The conductivity trends follow the Vogel—Fulcher—Tammann equation:

$$\sigma(T) = \sigma_{\infty} \exp\left(-\frac{DT_0}{T - T_0}\right) \tag{2}$$

where σ_{∞} is the high-temperature conductivity, T_0 is the Vogel temperature, and D is the strength parameter. The fit parameters for the thickest films are listed in Table 1, and the rest of the data are listed in Table S2. We considered the properties of the thickest PIL films the same as that of the bulk materials, and this was confirmed using a separate batch of PILs and measuring the thru-plane conductivities of 140 μ m thick films using two stainless-steel electrodes (Figure S4). In addition, it has been demonstrated previously for salt-blended polymer electrolyte films 39,40 that impedance measurements using IDEs do produce the same measured ionic conductivity value as bulk, parallel plate measurements when films are sufficiently thick.

The VFT parameters are analyzed as a function of thickness in Figure 2. It was found the D parameter slightly decreased in both BF₄ PILs while the trend is less obvious in TFSI PILs. The $T_{\rm g,bulk}-T_0$ values varied widely from approximately 40 to 90 K, and significant changes in $T_{\rm g,bulk}-T_0$ vs thickness were observed in BF₄ PILs. This is attributed to $T_{\rm g}$ -confinement

effects where the thin film $T_{\rm g}$ ($T_{\rm g,thin\ film}$) is higher than $T_{\rm g,bulk}$. A detailed discussion and its correlation with the conductivity drop under confinement are presented later. Here we also define a conductivity fragility ($m_{\rm cond}$) which is adopted from the fragility defined for structural relaxation. ¹³

$$m_{\text{cond}} = -\frac{\mathrm{d}(\log \sigma)}{\mathrm{d}(T_{g}/T)} \bigg|_{T=T_{g}} = \frac{DT_{0}T^{2}}{(T-T_{0})^{2}T_{g}\ln(10)} \bigg|_{T=T_{g}}$$

$$= \frac{DT_{0}T_{g}}{(T_{g}-T_{0})^{2}\ln(10)}$$
(3)

The negative sign in front of the derivative is to account for the negative slopes of the conductivity- T_{o}/T curves. This fragility parameter is used to quantify the rate of conductivity decrease with respect to the temperature drop near $T_{\rm e}$. The fragility parameter correlates with not only the strength parameter but also T_g and T_0 . We found that m_{cond} slightly increased with decreasing thickness for the Im BF₄ PIL. This suggests that the conductivity of BF4 PILs decreases much faster in thin films than in thick films as the temperature decreases. However, no obvious trend was observed for the other three PILs (Figure 2c). In the thickest films (i.e., bulk state), the TFSI PILs, which have higher m_{cond} , showed lower $T_{\rm g}$, which has been observed in some PILs (Table S3).^{41–43} It is noteworthy that this is opposite to the observed trends in structural relaxation fragility for neutral polymers⁴⁴ and one set of PILs with different pendant groups, 45 where fragilities were derived from rheology or dielectric spectroscopy. It needs to be stressed that m_{cond} reflects changes in conductivity rather than the underlying segmental dynamics, the two of which may be

coupled, but the segmental motion is more reflected in structural/dynamic fragility m. 46

The effect of film thickness on PIL conductivity at 100 $^{\circ}$ C is shown in Figure 3 where the data are normalized to the

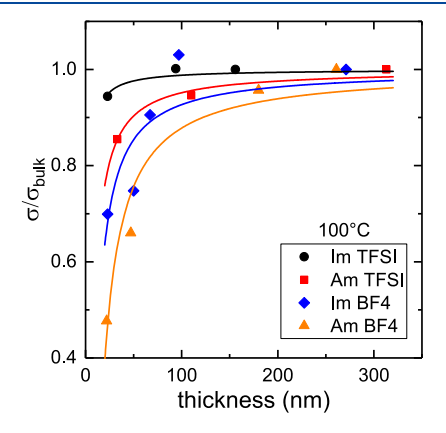


Figure 3. Ionic conductivity normalized to the thickest film of each PIL vs film thickness at 100 °C. Conductivity decreased as PIL film thickness approached 70 nm or below. The extent of conductivity drop for the thinnest film follows the trend Im TFSI < Am TFSI < Im BF $_4$ < Am BF $_4$. The solid curves are fits based on the bilayer conductivity model.

conductivity of the thickest film (>150 nm). The BF₄ PILs showed large drops (30% and 52% for imidazolium and ammonium cations, respectively) in conductivity as the film thickness decreased to around 30 nm, while the TFSI PILs only dropped 6% and 15%, respectively. Upon confinement, an increasing interface to bulk ratio leads to a greater importance of charge-surface interaction. Prior broadband dielectric measurements on a PIL³⁰ found that the ion dynamic rate slowed as the thickness approached 60 nm or below, and it was attributed to the increasing role of surface interactions. However, the extent of this interfacial effect was not quantified. A similar phenomenon was observed in a PIL simulation work by Yu et al., 31 and in-plane mean square displacement data showed that the anion diffusion was much slower in the first anion layer near the quartz substrate, whether the surface was neutral or negatively charged. Here we found that the extent of confinement correlated with the charge interaction strength where PILs with smaller, tighter binding ions like ammonium

cations or BF_4 anions were affected more than PILs with bulkier imidazolium and TFSI ions.

To quantify the interfacial effect, we used a two-layer conductivity model³⁹ to fit the normalized conductivity data:

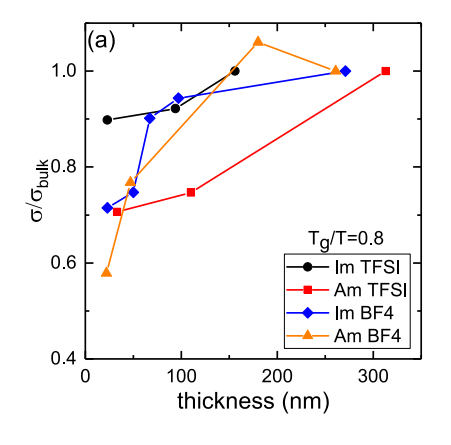
$$\frac{\sigma}{\sigma_{\text{bulk}}} = \frac{h - h_{\text{int}}}{h} \tag{4}$$

The bilayer model assumes that the interfacial layer has negligible conductivity compared to the bulk conductivity, and $h_{\rm int}$ is the interfacial layer thickness which is the parameter of interest. The fits are shown in Figure 3 and reasonably capture trends, although they are not exact due to the simplicity of the model. The $h_{\rm int}$ data are summarized in Table 1; $h_{\rm int}$ systematically increased from 1 to 12 nm as the IL pair changed from Im TFSI to Am BF₄. Based on the ion binding energy data of imidazolium ILs⁴⁷ and the $T_{\rm g}$ trend of the four PILs in this work, we think the ionic interaction strength follows the order Im TFSI < Im BF₄ < Am TFSI < Am BF₄. This suggested that the stronger ion pairs have stronger interaction with a solid surface, thus resulting in greater restriction of the anion motion.

Ionic conductivity normalized to bulk $T_{\rm g}$ (i.e., $T_{\rm g,bulk}/T=0.8$) is plotted against film thickness in Figure 4a to eliminate any difference between a fixed temperature and the PIL's bulk $T_{\rm g}$. The trend of conductivity decreasing under confinement is preserved relative to the trends in Figure 3, where Am BF₄ PIL showed a 42% decrease and Im TFSI PIL showed a 10% decrease. The Im BF₄ and Am TFSI PILs exhibited similar drops in conductivity (29%). The TFSI PILs have higher $m_{\rm cond}$ values, indicating the conductivity drop when approaching $T_{\rm g}$ is much steeper than that of the BF₄ PILs. To directly relate the conductivity fragility to this $T_{\rm g}$ -corrected conductivity, we calculated the VFT curve slopes at $T_{\rm g}/T=0.8$ (Table 1) based on eq 5:

$$s_{T_g/T=0.8} = -\frac{\mathrm{d}(\log \sigma)}{\mathrm{d}(T_g/T)} \bigg|_{T_g/T=0.8}$$

$$= \frac{DT_0T^2}{(T - T_0)^2 T_g \ln(10)} \bigg|_{T_g/T=0.8} = \frac{DT_0T_g}{(T_g - 0.8T_0)^2 \ln(10)}$$
(5)



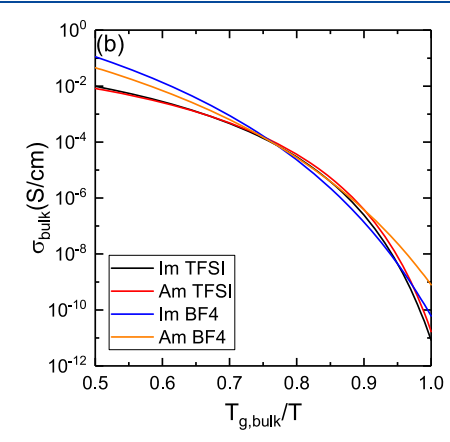


Figure 4. (a) Normalized conductivity of four PILs vs film thickness at $T_{\rm g,bulk}/T = 0.8$. (b) VFT fit curves of bulk conductivity vs temperature for four PILs on a $T_{\rm g}$ normalized scale, illustrating different rates of conductivity drop (i.e., fragility) at a fixed $T_{\rm g}/T$.

It can be seen from Figure 4b that when m_{cond} is large (i.e., a steeper slope at $T_g/T = 1$), the curve slope far away from T_g will be small. This is the case for TFSI PILs at $T_{\rm g}/T=0.8$. At this temperature, the conductivity of the TFSI PILs is less sensitive to changes in temperature or $T_{\rm g}$. When the polymer T_g increases with reducing thickness, the relative change between T and T_g will only induce a small conductivity drop. In short, higher m_{cond} PILs will have a smaller VFT slope at T $\gg T_{\sigma}$ and show a smaller conductivity confinement effect. Conversely, the larger conductivity drop in BF₄ PILs is due to their smaller m_{cond} . The conductivity change can be further analyzed by quantifying the differences in the $T_{\rm g}$ ($\Delta T_{\rm g}$ = $T_{\rm g,thin~film}$ – $T_{\rm g,bulk}$) with and without confinement. The VFT equation of the bulk material was modified, and the measured conductivity values of the thin films were used to calculate a hypothetical thin film temperature. The difference between this hypothetical temperature and the actual measured temperature can be approximated as $\Delta T_{\rm g}$. The calculation procedure is demonstrated in the Supporting Information, and the data are plotted as a function of film thickness in Figure S5. The estimated T_{σ} increase varied from 1 to 7 K in this study. This is similar to or smaller than the observed T_g increase in systems with substantial material-surface interactions, such as poly-(methyl methacrylate) thin films on silica substrates, 48,49 polystyrene (PS) thin films on high interfacial energy substrates, 50 PS infiltrated into silica nanoparticle films, 51 and small-molecule ionic liquids confined in alumina⁵² or silica⁵³ nanopores. It is noteworthy that in neutral polymer thin film confinement studies, there is a competing effect between the polymer-free surface interaction, which generally leads to a decrease in $T_{g'}^{54-58}$ and the attractive polymer–substrate interaction mentioned earlier, which tends to increase $T_{\rm g}^{59,60}$ However, the relative strength of these two interactions is still not clear in the ionic polymers, and an experimental study on the T_{g} confinement effect in PILs is needed in the future to elucidate the polymer dynamics.

The dielectric loss $(\tan(\delta))$ and the real component of the conductivity (σ') of PIL thin films with different thicknesses were analyzed as a function of frequency at 100 °C. The results are shown in Figure 5 and Figure S6. The $\tan(\delta)$ response can

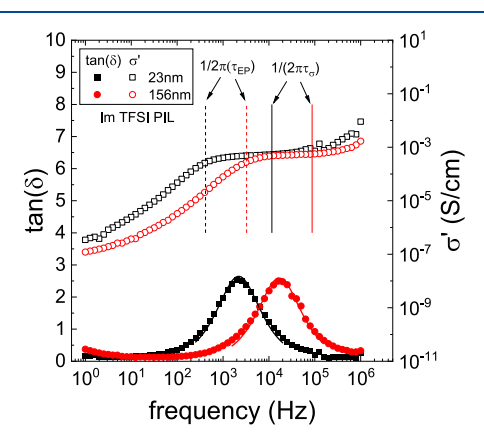


Figure 5. Dielectric loss $\tan(\delta)$ (solid symbols) and real conductivity (empty symbols) vs frequency at 100 °C for Im TFSI PIL with two different thicknesses (black, 24 nm; red, 156 nm). The solid curves are $\tan(\delta)$ fits. The dash and solid straight lines are the frequencies of electrode polarization and ion diffusion process, respectively. The $\tan(\delta)$ peak shifted to lower frequency, and two characteristic relaxation times increased with decreasing thickness.

be fit to the electrode polarization (EP) model for single ion conductors as described in Klein et al.:⁶¹

$$\tan \delta = \frac{\omega \tau_{\rm EP}}{1 + \omega^2 \tau_{\sigma} \tau_{\rm EP}} \tag{6}$$

where $\tau_{\rm EP}$ is the time scale where ions start to accumulate and polarize at the blocking electrode and τ_{σ} is the time scale where ion motion becomes diffusive. In the σ' plot, $\tau_{\rm EP}$ is related to the onset of the conductivity decrease in the low-frequency regime, and τ_{σ} corresponds to the onset of the σ' plateau in the high-frequency regime. The fit results are shown in Table S2. The $\tan(\delta)$ peak, as well as two relaxation times, systematically shifted to lower frequency as the film thickness decreased. Due to the geometric difference betweenthe IDE and the parallel plate, the origins of these frequency shifts need to be interpreted differently. Recalled from Klein et al., 61 for the parallel plate geometry

$$\tau_{\rm EP} = \frac{\varepsilon_{\rm EP}}{\sigma} \tag{7}$$

$$\tau_{\sigma} = \frac{\varepsilon_{\rm R}}{\sigma} \tag{8}$$

where σ is the ionic conductivity, $\varepsilon_{\rm EP}$ is the polymer permittivity with electrode polarization, and $\varepsilon_{\rm R}$ is the permittivity without electrode polarization. These relaxation times are directly related to different RC constants from equivalent circuit analysis of the impedance data, which was demonstrated in Sharon et al. ⁴⁰ Briefly, in the IDE geometry

$$\tau_{\rm EP} = R_{\rm film} C_{\rm int} = \left(\frac{1}{\sigma} \frac{d}{(N-1)lh}\right) \left(\varepsilon_{\rm EP} \frac{A_{\rm electrode}}{d}\right) \sim \frac{\varepsilon_{\rm EP}}{\sigma} \left(\frac{1}{h}\right)$$
(9)

$$\tau_{\sigma} = R_{\text{film}} C_{\text{film}} = \left(\frac{1}{\sigma} \frac{d}{(N-1)lh}\right) \left(\varepsilon_{R} \frac{(N-1)lh}{d}\right) = \frac{\varepsilon_{R}}{\sigma}$$
(10)

where $A_{\rm electrode}$ is the surface area of gold electrodes, and it is a constant. The EP time should be film thickness dependent in the IDE configuration, and experimentally we observed that $\tau_{\rm EP}$ increased with decreasing film thickness. For the geometry-independent τ_{σ} , we found that the decreasing conductivity under confinement contributed to the slowdown of ion diffusion in the polymer thin films. The increasing τ_{σ} also supports the argument that thin film confinement results in elevated $T_{\rm g}$ in PILs since the ion motion is coupled to the segmental dynamics to some degree.

CONCLUSION

Four pendant PILs with the same acrylate backbone but different IL groups were synthesized. The ion interaction was tuned by pairing ammonium or imidazolium cations with BF₄ or TFSI anions. The bulk glass transition temperature of PILs increased as follows: Im TFSI < Am TFSI < Im BF₄ < Am BF₄, which is a good indicator of the binding energy of the ion pairs. 47,62 Ionic polymer thin films with thickness ranging from 23 to 313 nm were prepared by spin coating onto interdigitated gold electrodes to examine the confinement effect on ion transport. The ionic conductivity decreased when the PIL thickness was below 70 nm. The confinement effect was attributed to the charge—substrate interaction and a possible $T_{\rm g}$ increase due to nanoconfinement which hinders

ion transport. The strongest IL pair (Am BF₄) showed the most conductivity drop while the weakest IL pair (Im TFSI) showed the least conductivity drop. The difference is possibly due to variations in interfacial layer thickness, based on the two-layer model fits. The extent of confinement is correlated to the conductivity fragility $m_{\rm cond}$ from the VFT fits, where BF₄ PILs with smaller conductivity fragility would experience a sharper conductivity drop at a fixed $T_{\rm g}/T$, when the PIL $T_{\rm g}$ increases with confinement. The TFSI PILs, on the other hand, have larger $m_{\rm cond}$, and the conductivity drop is less intense at a fixed $T_{\rm g}/T$. In addition, the dielectric loss peak shifted to lower frequency as the film thickness decreased, indicating a slowdown of the ion diffusion process, which is related to conductivity and $T_{\rm g}$ confinement effects in PILs.

ASSOCIATED CONTENT

Supporting Information

The Supporting Information is available free of charge at https://pubs.acs.org/doi/10.1021/acs.macromol.1c01820.

PIL synthesis and characterization procedures, PIL NMR spectra, DSC curves, optical image of a PIL thin film, conductivity comparison, $\Delta T_{\rm g}$ calculation, elemental analysis results, VFT fit parameters, and electrode polarization analysis results (PDF)

AUTHOR INFORMATION

Corresponding Authors

Christopher M. Evans — Department of Materials Science and Engineering and Beckman Institute for Advanced Science and Technology, University of Illinois at Urbana—Champaign, Urbana, Illinois 61801, United States; orcid.org/0000-0003-0668-2500; Email: shrayesh@uchicago.edu

Shrayesh N. Patel — Pritzker School of Molecular Engineering, University of Chicago, Chicago, Illinois 60637, United States; orcid.org/0000-0003-3657-827X; Email: cme365@illinois.edu

Authors

Qiujie Zhao – Department of Materials Science and Engineering, University of Illinois at Urbana–Champaign, Urbana, Illinois 61801, United States

Peter Bennington – Pritzker School of Molecular Engineering, University of Chicago, Chicago, Illinois 60637, United States; © orcid.org/0000-0002-0501-1441

Paul F. Nealey — Pritzker School of Molecular Engineering, University of Chicago, Chicago, Illinois 60637, United States; Materials Science Division, Argonne National Laboratory, Lemont, Illinois 60439, United States; orcid.org/0000-0003-3889-142X

Complete contact information is available at: https://pubs.acs.org/10.1021/acs.macromol.1c01820

Notes

The authors declare no competing financial interest.

ACKNOWLEDGMENTS

This work is funded by the National Science Foundation (NSF) under award DMR-1751291. Part of the research was carried out in the Materials Research Laboratory (MRL), the Microanalysis Laboratory, and the NMR Laboratory at the University of Illinois, Urbana—Champaign. This work made use of the Pritzker Nanofabrication Facility, which receives

partial support from the SHyNE Resource, a node of the National Science Foundation's National Nanotechnology Coordinated Infrastructure (NSF ECCS-2025633). This work made use of the shared facilities at the University of Chicago Materials Research Science and Engineering Center, supported by the National Science Foundation under award number DMR-2011854. P. B. and P. F. N. acknowledge support from the U.S. Department of Energy (DOE) Basic Energy Sciences, Materials Science and Engineering Division for the thin film conductivity measurements.

REFERENCES

- (1) Ohno, H. Electrochemical aspects of ionic liquids; John Wiley & Sons, Inc.: Hoboken, NJ, 2005.
- (2) Eftekhari, A.; Saito, T. Synthesis and properties of polymerized ionic liquids. Eur. Polym. J. 2017, 90, 245–272.
- (3) Nykaza, J. R.; Savage, A. M.; Pan, Q.; Wang, S.; Beyer, F. L.; Tang, M. H.; Li, C. Y.; Elabd, Y. A. Polymerized ionic liquid diblock copolymer as solid-state electrolyte and separator in lithium-ion battery. *Polymer* **2016**, *101*, 311–318.
- (4) Porcarelli, L.; Shaplov, A. S.; Bella, F.; Nair, J. R.; Mecerreyes, D.; Gerbaldi, C. Single-Ion Conducting Polymer Electrolytes for Lithium Metal Polymer Batteries that Operate at Ambient Temperature. *ACS Energy Letters* **2016**, *1* (4), 678–682.
- (5) de Oliveira, P. S. C.; Alexandre, S. A.; Silva, G. G.; Trigueiro, J. P. C.; Lavall, R. L. PIL/IL gel polymer electrolytes: The influence of the IL ions on the properties of solid-state supercapacitors. *Eur. Polym. J.* **2018**, *108*, 452–460.
- (6) Trigueiro, J. P. C.; Lavall, R. L.; Silva, G. G. Supercapacitors based on modified graphene electrodes with poly(ionic liquid). *J. Power Sources* **2014**, 256, 264–273.
- (7) Shen, C.; Zhao, Q.; Evans, C. M. Precise Network Polymerized Ionic Liquids for Low-Voltage, Dopant-Free Soft Actuators. *Advanced Materials Technologies* **2019**, 4 (2), 1800535.
- (8) Kim, O.; Kim, H.; Choi, U. H.; Park, M. J. One-volt-driven superfast polymer actuators based on single-ion conductors. *Nat. Commun.* **2016**, *7*, 13576.
- (9) Wang, Y.; Fan, F.; Agapov, A. L.; Saito, T.; Yang, J.; Yu, X.; Hong, K.; Mays, J.; Sokolov, A. P. Examination of the fundamental relation between ionic transport and segmental relaxation in polymer electrolytes. *Polymer* **2014**, *55* (16), 4067–4076.
- (10) Hemp, S. T.; Zhang, M.; Allen, M. H.; Cheng, S.; Moore, R. B.; Long, T. E. Comparing Ammonium and Phosphonium Polymerized Ionic Liquids: Thermal Analysis, Conductivity, and Morphology. *Macromol. Chem. Phys.* **2013**, *214* (18), 2099–2107.
- (11) Ye, Y.; Elabd, Y. A. Anion exchanged polymerized ionic liquids: High free volume single ion conductors. *Polymer* **2011**, *52* (5), 1309–1317.
- (12) Evans, C. M.; Bridges, C. R.; Sanoja, G. E.; Bartels, J.; Segalman, R. A. Role of Tethered Ion Placement on Polymerized Ionic Liquid Structure and Conductivity: Pendant versus Backbone Charge Placement. ACS Macro Lett. 2016, 5 (8), 925–930.
- (13) Kuray, P.; Noda, T.; Matsumoto, A.; Iacob, C.; Inoue, T.; Hickner, M. A.; Runt, J. Ion Transport in Pendant and Backbone Polymerized Ionic Liquids. *Macromolecules* **2019**, 52 (17), 6438–6448
- (14) Jourdain, A.; Serghei, A.; Drockenmuller, E. Enhanced Ionic Conductivity of a 1,2,3-Triazolium-Based Poly(siloxane ionic liquid) Homopolymer. ACS Macro Lett. 2016, 5 (11), 1283–1286.
- (15) Wojnarowska, Z.; Feng, H.; Fu, Y.; Cheng, S.; Carroll, B.; Kumar, R.; Novikov, V. N.; Kisliuk, A. M.; Saito, T.; Kang, N.-G.; Mays, J. W.; Sokolov, A. P.; Bocharova, V. Effect of Chain Rigidity on the Decoupling of Ion Motion from Segmental Relaxation in Polymerized Ionic Liquids: Ambient and Elevated Pressure Studies. *Macromolecules* **2017**, *50* (17), *6710–6721*.
- (16) Zhao, Q.; Shen, C.; Halloran, K. P.; Evans, C. M. Effect of Network Architecture and Linker Polarity on Ion Aggregation and

- Conductivity in Precise Polymerized Ionic Liquids. ACS Macro Lett. 2019, 8 (6), 658-663.
- (17) Lee, M.; Choi, U. H.; Colby, R. H.; Gibson, H. W. Ion Conduction in Imidazolium Acrylate Ionic Liquids and their Polymers. *Chem. Mater.* **2010**, 22 (21), 5814–5822.
- (18) Maruyama, S.; Prastiawan, I. B. H.; Toyabe, K.; Higuchi, Y.; Koganezawa, T.; Kubo, M.; Matsumoto, Y. Ionic Conductivity in Ionic Liquid Nano Thin Films. *ACS Nano* **2018**, *12* (10), 10509–10517.
- (19) Garaga, M. N.; Aguilera, L.; Yaghini, N.; Matic, A.; Persson, M.; Martinelli, A. Achieving enhanced ionic mobility in nanoporous silica by controlled surface interactions. *Phys. Chem. Chem. Phys.* **2017**, *19* (8), 5727–5736.
- (20) Tu, W.; Chat, K.; Szklarz, G.; Laskowski, L.; Grzybowska, K.; Paluch, M.; Richert, R.; Adrjanowicz, K. Dynamics of Pyrrolidinium-Based Ionic Liquids under Confinement. II. The Effects of Pore Size, Inner Surface, and Cationic Alkyl Chain Length. *J. Phys. Chem. C* **2020**, *124* (9), 5395–5408.
- (21) Iacob, C.; Sangoro, J. R.; Kipnusu, W. K.; Valiullin, R.; Kärger, J.; Kremer, F. Enhanced charge transport in nano-confined ionic liquids. *Soft Matter* **2012**, *8* (2), 289–293.
- (22) Richter, D.; Kruteva, M. Polymer dynamics under confinement. Soft Matter 2019, 15 (37), 7316–7349.
- (23) Evans, C. M.; Sanoja, G. E.; Popere, B. C.; Segalman, R. A. Anhydrous Proton Transport in Polymerized Ionic Liquid Block Copolymers: Roles of Block Length, Ionic Content, and Confinement. *Macromolecules* **2016**, *49* (1), 395–404.
- (24) Ye, Y.; Choi, J.-H.; Winey, K. I.; Elabd, Y. A. Polymerized Ionic Liquid Block and Random Copolymers: Effect of Weak Microphase Separation on Ion Transport. *Macromolecules* **2012**, *45* (17), 7027–7035.
- (25) Ye, Y.; Sharick, S.; Davis, E. M.; Winey, K. I.; Elabd, Y. A. High Hydroxide Conductivity in Polymerized Ionic Liquid Block Copolymers. ACS Macro Lett. 2013, 2 (7), 575–580.
- (26) Weber, R. L.; Ye, Y.; Schmitt, A. L.; Banik, S. M.; Elabd, Y. A.; Mahanthappa, M. K. Effect of Nanoscale Morphology on the Conductivity of Polymerized Ionic Liquid Block Copolymers. *Macromolecules* **2011**, *44* (14), 5727–5735.
- (27) Choi, J.-H.; Ye, Y.; Elabd, Y. A.; Winey, K. I. Network Structure and Strong Microphase Separation for High Ion Conductivity in Polymerized Ionic Liquid Block Copolymers. *Macromolecules* **2013**, 46 (13), 5290–5300.
- (28) Kinsey, T.; Glynn, K.; Cosby, T.; Iacob, C.; Sangoro, J. Ion Dynamics of Monomeric Ionic Liquids Polymerized In Situ within Silica Nanopores. *ACS Appl. Mater. Interfaces* **2020**, *12* (39), 44325–44334.
- (29) Tarnacka, M.; Chrobok, A.; Matuszek, K.; Golba, S.; Maksym, P.; Kaminski, K.; Paluch, M. Polymerization of Monomeric Ionic Liquid Confined within Uniaxial Alumina Pores as a New Way of Obtaining Materials with Enhanced Conductivity. ACS Appl. Mater. Interfaces 2016, 8 (43), 29779–29790.
- (30) Heres, M.; Cosby, T.; Mapesa, E. U.; Sangoro, J. Probing Nanoscale Ion Dynamics in Ultrathin Films of Polymerized Ionic Liquids by Broadband Dielectric Spectroscopy. *ACS Macro Lett.* **2016**, 5 (9), 1065–1069.
- (31) Yu, Z.; Fang, C.; Huang, J.; Sumpter, B. G.; Qiao, R. Molecular Structure and Dynamics of Interfacial Polymerized Ionic Liquids. *J. Phys. Chem. C* **2018**, *122* (39), 22494–22503.
- (32) Shan, N.; Shen, C.; Evans, C. M. Critical Role of Ion Exchange Conditions on the Properties of Network Ionic Polymers. *ACS Macro Lett.* **2020**, *9*, 1718–1725.
- (33) Zhao, Q.; Evans, C. M. Effect of Molecular Weight on Viscosity Scaling and Ion Transport in Linear Polymerized Ionic Liquids. *Macromolecules* **2021**, *54* (7), 3395–3404.
- (34) Fan, F.; Wang, W.; Holt, A. P.; Feng, H.; Uhrig, D.; Lu, X.; Hong, T.; Wang, Y.; Kang, N.-G.; Mays, J.; Sokolov, A. P. Effect of Molecular Weight on the Ion Transport Mechanism in Polymerized Ionic Liquids. *Macromolecules* **2016**, *49* (12), 4557–4570.

- (35) Jin, S.; McKenna, G. B. Effect of Nanoconfinement on Polymer Chain Dynamics. *Macromolecules* **2020**, 53 (22), 10212–10216.
- (36) Choi, U. H.; Lee, M.; Wang, S.; Liu, W.; Winey, K. I.; Gibson, H. W.; Colby, R. H. Ionic Conduction and Dielectric Response of Poly(imidazolium acrylate) Ionomers. *Macromolecules* **2012**, *45* (9), 3974–3985.
- (37) Morozova, S. M.; Shaplov, A. S.; Lozinskaya, E. I.; Vlasov, P. S.; Sardon, H.; Mecerreyes, D.; Vygodskii, Y. S. Poly(ionic liquid)-based polyurethanes having imidazolium, ammonium, morpholinium or pyrrolidinium cations. *High Perform. Polym.* **2017**, 29 (6), 691–703.
- (38) Sharon, D.; Bennington, P.; Dolejsi, M.; Webb, M. A.; Dong, B. X.; de Pablo, J. J.; Nealey, P. F.; Patel, S. N. Intrinsic Ion Transport Properties of Block Copolymer Electrolytes. *ACS Nano* **2020**, *14* (7), 8902–8914.
- (39) Dong, B. X.; Bennington, P.; Kambe, Y.; Sharon, D.; Dolejsi, M.; Strzalka, J.; Burnett, V. F.; Nealey, P. F.; Patel, S. N. Nanothin film conductivity measurements reveal interfacial influence on ion transport in polymer electrolytes. *Molecular Systems Design & Engineering* 2019, 4 (3), 597–608.
- (40) Sharon, D.; Bennington, P.; Liu, C.; Kambe, Y.; Dong, B. X.; Burnett, V. F.; Dolejsi, M.; Grocke, G.; Patel, S. N.; Nealey, P. F. Interrogation of Electrochemical Properties of Polymer Electrolyte Thin Films with Interdigitated Electrodes. *J. Electrochem. Soc.* **2018**, 165 (16), H1028—H1039.
- (41) Shen, C.; Zhao, Q.; Evans, C. M. Ion specific, odd-even glass transition temperatures and conductivities in precise network polymerized ionic liquids. *Molecular Systems Design & Engineering* **2019**, *4* (2), 332–341.
- (42) Arora, S.; Rozon, J.; Lasser, J. E. Dynamics of Ion Locking in Doubly-Polymerized Ionic Liquids. *Macromolecules* **2021**, *54* (13), 6466–6476.
- (43) Choi, U. H.; Ye, Y.; Salas de la Cruz, D.; Liu, W.; Winey, K. I.; Elabd, Y. A.; Runt, J.; Colby, R. H. Dielectric and Viscoelastic Responses of Imidazolium-Based Ionomers with Different Counterions and Side Chain Lengths. *Macromolecules* **2014**, *47* (2), 777–790.
- (44) Qin, Q.; McKenna, G. B. Correlation between dynamic fragility and glass transition temperature for different classes of glass forming liquids. *J. Non-Cryst. Solids* **2006**, 352 (28–29), 2977–2985.
- (45) Fan, F.; Wang, Y.; Hong, T.; Heres, M. F.; Saito, T.; Sokolov, A. P. Ion Conduction in Polymerized Ionic Liquids with Different Pendant Groups. *Macromolecules* **2015**, *48* (13), 4461–4470.
- (46) Angell, C. A. Formation of Glasses from Liquids and Biopolymers. *Science* **1995**, 267 (5206), 1924–1935.
- (47) Hunt, P. A.; Gould, I. R.; Kirchner, B. The Structure of Imidazolium-Based Ionic Liquids: Insights From Ion-Pair Interactions. *Aust. J. Chem.* **2007**, *60* (1), 9.
- (48) Mundra, M. K.; Donthu, S. K.; Dravid, V. P.; Torkelson, J. M. Effect of Spatial Confinement on the Glass-Transition Temperature of Patterned Polymer Nanostructures. *Nano Lett.* **2007**, *7* (3), 713–718.
- (49) Keddie, J. L.; Jones, R. A. L.; Cory, R. A. Interface and surface effects on the glass-transition temperature in thin polymer films. *Faraday Discuss.* **1994**, 98 (0), 219–230.
- (50) Fryer, D. S.; Peters, R. D.; Kim, E. J.; Tomaszewski, J. E.; de Pablo, J. J.; Nealey, P. F.; White, C. C.; Wu, W.-l. Dependence of the Glass Transition Temperature of Polymer Films on Interfacial Energy and Thickness. *Macromolecules* **2001**, 34 (16), 5627–5634.
- (51) Wang, H.; Hor, J. L.; Zhang, Y.; Liu, T.; Lee, D.; Fakhraai, Z. Dramatic Increase in Polymer Glass Transition Temperature under Extreme Nanoconfinement in Weakly Interacting Nanoparticle Films. *ACS Nano* **2018**, *12* (6), 5580–5587.
- (52) Zuo, Y.; Zhang, Y.; Huang, R.; Min, Y. The effect of nanoconfinement on the glass transition temperature of ionic liquids. *Phys. Chem. Chem. Phys.* **2019**, *21* (1), 22–25.
- (53) Gupta, A. K.; Verma, Y. L.; Singh, R. K.; Chandra, S. Studies on an Ionic Liquid Confined in Silica Nanopores: Change inTgand Evidence of Organic–Inorganic Linkage at the Pore Wall Surface. *J. Phys. Chem. C* **2014**, *118* (3), 1530–1539.
- (\$4) Forrest, J. A.; Dalnoki-Veress, K.; Dutcher, J. R. Interface and chain confinement effects on the glass transition temperature of thin

- polymer films. Phys. Rev. E: Stat. Phys., Plasmas, Fluids, Relat. Interdiscip. Top. 1997, 56 (5), 5705-5716.
- (55) Dalnoki-Veress, K.; Forrest, J. A.; de Gennes, P. G.; Dutcher, J. R. Glass transition reductions in thin freely-standing polymer films: A scaling analysis of chain confinement effects. *J. Phys. IV* **2000**, *10* (PR7), Pr7-221–Pr7-226.
- (56) Ellison, C. J.; Torkelson, J. M. Sensing the glass transition in thin and ultrathin polymer films via fluorescence probes and labels. *J. Polym. Sci., Part B: Polym. Phys.* **2002**, *40* (24), 2745–2758.
- (57) Ellison, C. J.; Mundra, M. K.; Torkelson, J. M. Impacts of Polystyrene Molecular Weight and Modification to the Repeat Unit Structure on the Glass Transition—Nanoconfinement Effect and the Cooperativity Length Scale. *Macromolecules* **2005**, 38 (5), 1767—1778.
- (58) Kim, J. H.; Jang, J.; Zin, W.-C. Thickness Dependence of the Glass Transition Temperature in Thin Polymer Films. *Langmuir* **2001**, *17* (9), 2703–2710.
- (59) van Zanten, J. H.; Wallace, W. E.; Wu, W.-l. Effect of strongly favorable substrate interactions on the thermal properties of ultrathin polymer films. *Phys. Rev. E: Stat. Phys., Plasmas, Fluids, Relat. Interdiscip. Top.* **1996**, 53 (3), R2053–R2056.
- (60) Park, C. H.; Kim, J. H.; Ree, M.; Sohn, B.-H.; Jung, J. C.; Zin, W.-C. Thickness and composition dependence of the glass transition temperature in thin random copolymer films. *Polymer* **2004**, *45* (13), 4507–4513.
- (61) Klein, R. J.; Zhang, S.; Dou, S.; Jones, B. H.; Colby, R. H.; Runt, J. Modeling electrode polarization in dielectric spectroscopy: Ion mobility and mobile ion concentration of single-ion polymer electrolytes. *J. Chem. Phys.* **2006**, *124* (14), 144903.
- (62) Siqueira, L. J. A.; Ribeiro, M. C. C. Alkoxy Chain Effect on the Viscosity of a Quaternary Ammonium Ionic Liquid: Molecular Dynamics Simulations. *J. Phys. Chem. B* **2009**, *113* (4), 1074–1079.